molbank

MDPI

Communication

Structural Elucidation of 2-(6-(Diethylamino)benzofuran-2-yl)-3-hydroxy-4*H*-chromen-4-one and Labelling of *Mycobacterium aurum* Cells

Adrian Richter [1], Richard Goddard [2], Fabienne Siersleben [1], Lea Mann [1] and Rüdiger W. Seidel [1,*]

[1] Institute of Pharmacy, Martin Luther University Halle-Wittenberg, Wolfgang-Langenbeck-Straße 4, 06120 Halle (Saale), Germany; adrian.richter@pharmazie.uni-halle.de (A.R.); fabienne.siersleben@pharmazie.uni-halle.de (F.S.); lea.mann@pharmazie.uni-halle.de (L.M.)
[2] Max-Planck-Institut für Kohlenforschung, Kaiser-Wilhelm-Platz 1, 45470 Mülheim an der Ruhr, Germany; goddard@mpi-muelheim.mpg.de
* Correspondence: ruediger.seidel@pharmazie.uni-halle.de; Tel.: +49-345-552-5154

Abstract: Trehalose conjugates of 3-hydroxychromone (3HC) dyes have previously been utilized as fluorescence labels to detect metabolically active mycobacteria with a view to facilitating point-of-care detection of mycobacterial pathogens, especially *Mycobacterium tuberculosis*. We subjected the 3HC dye 2-(6-(diethylamino)benzofuran-2-yl)-3-hydroxy-4*H*-chromen-4-one (**3HC-2**) to a combined X-ray crystallography and density functional theory (DFT) study, and conducted preliminary fluorescence labelling experiments with the model organism *Mycobacterium aurum*. In the crystal, **3HC-2** exhibits an s-*cis* conformation of the chromone and the benzofuran moieties about the central C–C bond. According to DFT calculations, the *s-cis* conformer is about 1.8 kcal mol^{-1} lower in energy than the *s-trans* conformer. The solid-state supramolecular structure features hydrogen-bonded dimers and $\pi\cdots\pi$ stacking. Fluorescence microscopy revealed fluorescence of *M. aurum* cells treated with the dye trehalose conjugate **3HC-2-Tre** in the GFP channel. It was concluded that s-*cis* is the preferred conformation of **3HC-2** and that the generally considered non-pathogenic *M. aurum* can be labelled with the fluorescence probe **3HC-2-Tre** for convenient in vitro drug screening of new antimycobacterial agents.

Keywords: 3-hydroxychromone; crystal structure; hydrogen bonding; Hirshfeld surface analysis; conformation; DFT calculation; fluorescence labelling; *Mycobacterium aurum*

Citation: Richter, A.; Goddard, R.; Siersleben, F.; Mann, L.; Seidel, R.W. Structural Elucidation of 2-(6-(Diethylamino)benzofuran-2-yl)-3-hydroxy-4*H*-chromen-4-one and Labelling of *Mycobacterium aurum* Cells. *Molbank* **2023**, *2023*, M1647. https://doi.org/10.3390/M1647

Academic Editor: Kristof Van Hecke

Received: 24 April 2023
Revised: 9 May 2023
Accepted: 11 May 2023
Published: 16 May 2023

1. Introduction

With a total of 1.6 million deaths and an estimate of 10.6 new cases worldwide in 2021, tuberculosis (TB) remains the leading bacterial killer and a public health threat [1]. The etiologic agent of TB is primarily *Mycobacterium tuberculosis*. Infections caused by non-tuberculous mycobacteria (NTM), which are mostly considered opportunistic pathogens, are also on the rise globally [2,3]. Point-of-care detection of mycobacteria based on low-cost microscopy methods [4] could help prevent and combat mycobacterial infections. In this context, Kamariza et al. recently reported on 3-hydroxychromone dye trehalose conjugates for the fluorescence labelling of mycobacterial cells [5]. As illustrated in Figure 1, exogenous trehalose molecules can be mycolylated at position 6 to give trehalose monomycolates (TMM), which are incorporated into the mycomembrane. A solvatochromic 3-hydroxychromone dye appended to trehalose as a fluorophore group appears to be tolerated by the converting enzymes antigene 85 (Ag85), which enables visualization of metabolically active mycobacteria.

Mycobacterium aurum is a fast-growing non-tuberculous mycobacterium [6], which has been used as a surrogate bacterium in anti-TB drug discovery [7–9], although its suitability as a model organism for *M. tuberculosis* has been called into question [10]. *M. aurum* is

generally considered non-pathogenic, but a documented rare case of keratitis attributable to *M. aurum* has been reported in the medical literature [11]. We have also used *M. aurum* as a test bacterium in early-stage antimycobacterial drug discovery [12–14]. Therefore, we became interested in possible applications of the fluorescence probe **3HC-2-Tre** (Figure 2) [5] for the labelling of *M. aurum* cells, as this could be a useful tool for in vitro testing of new antimycobacterial agents.

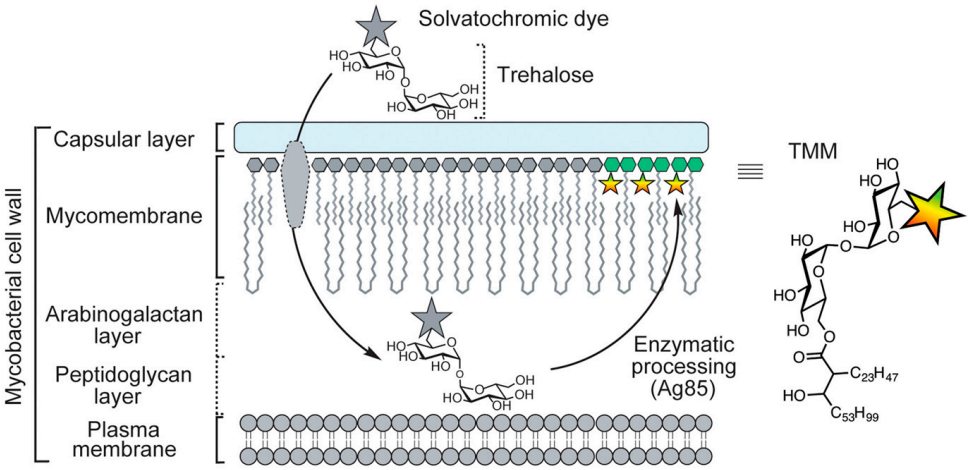

Figure 1. Simplified representation of the mycobacterial cell wall, illustrating the conversion of dye trehalose conjugates to the corresponding trehalose monomycolates (TMM, chemical diagram on the right) and insertion into the mycomembrane. The figure was adapted from Ref. [5]. Published Open Access under the Creative Commons Attribution 4.0 International License (https://creativecommons.org/licenses/by/4.0/ (accessed on 23 April 2023)). Copyright 2021 The Authors.

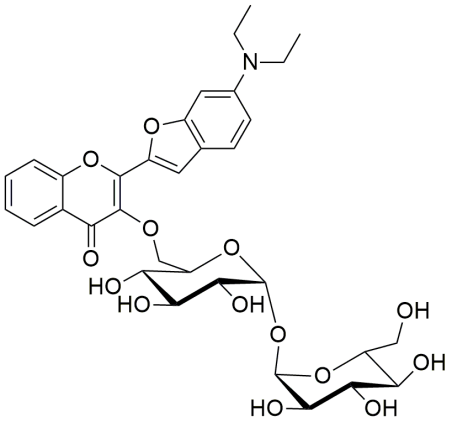

Figure 2. Chemical diagram of the dye trehalose conjugate **3HC-2-Tre** used in this study.

Whereas in-depth spectroscopic investigations of the dye **3HC-2** can be found in the literature [15,16], its crystal and molecular structure appears to be hitherto unpublished, as revealed by a search of the Cambridge Structural Database (CSD) [17] via the WebCSD interface [18] in April 2023. Therefore, we subjected **3HC-2** to X-ray crystallography, density functional theory (DFT) calculations, and Hirshfeld surface analysis in order to better understand its features. In this contribution, we report the molecular structure of **3HC-2** in the crystal, a computational study of its conformational preference, its supramolecular structure in the solid state, and the preliminary results of fluorescence labelling experiments with *M. aurum* cells using the dye trehalose conjugate **3HC-2-Tre**.

2. Results and Discussion

*2.1. Structural Description of **3HC-2***

Compound **3HC-2** (Figure 3a) was synthesized as described in the literature [5]. In brief, 2′-hydroxyacetophenone was reacted with 6-(diethylamino)benzofuran-2-carbaldehyde [16], followed by treatment with hydrogen peroxide to give the desired 3-hydroxychromone derivative **3HC-2**. Intense yellow crystals of **3HC-2**, as shown in Figure 3b, grew from a solution in heptane/ethyl acetate. X-ray crystallography revealed that the compound crystallized solvent-free in the triclinic system, centrosymmetric space group *P*-1, with two molecules in the unit cell ($Z = 2$).

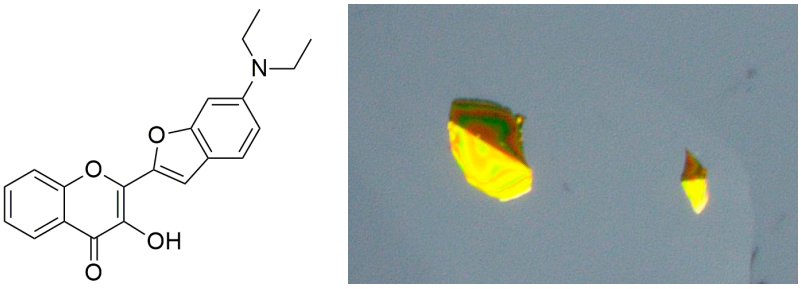

(**a**) (**b**)

Figure 3. Chemical diagram of **3HC-2** (**a**) and microscope image of crystal specimens in perfluoropolyether oil (**b**).

Figure 4 shows the molecular structure of **3HC-2** in the crystal. One of the ethyl groups exhibits disorder over two positions. As expected, the ten-membered chromene system is planar (r.m.s. deviation 0.0108 Å) as is the nine-membered benzofuran moiety tethered to C2 (r.m.s. deviation 0.0107 Å). The molecule adopts an s-*cis* conformation about the C2–C2′ bond. The O1–C2–C2′–O1′ torsion angle is −13.76(16)° in the chosen asymmetric unit, and the angle between the mean planes through the chromene and benzofuran moieties is 14.42(4)°. An s-*cis* conformation was encountered in the related 3-(furan-2-yl)-2-hydroxy-4*H*-chromen-4-one (CSD refcodes: IJUCEW and IJUCEW01) [19,20] and its nicotinic acid ester (MASGAS) [21]. Interestingly, an s-*trans* conformation was found in the crystal structures of the 2-thiophenyl derivatives ((5-(3-hydroxy-4-oxo-4*H*-chromen-2-yl)-2-thienyl)methylene)malononitrile (MUGGEC) [22] and 2-(thiophen-2-yl)-4*H*-chromen-4-one-3-*O*-2,3,4,6-*O*-tetraacetyl-*β*-D-glucopyranoside (QICLIA) [23].

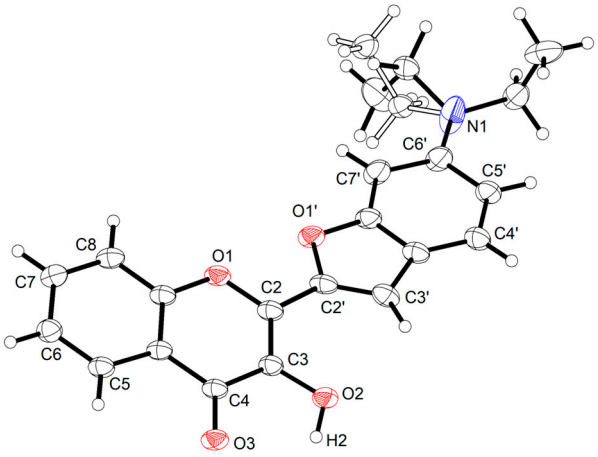

Figure 4. Displacement ellipsoid plot of **3HC-2** drawn at the 50% probability level. Hydrogen atoms are represented by small spheres of arbitrary radius. The part of the disordered ethyl group with minor occupancy (ca. 47%) is shown with empty bonds.

A CSD search (April 2023) for crystal structures containing a 2,3-diether-butadiene moiety with a central acyclic C-C single bond revealed 107 entries. Of these, 80 structures exhibited an O–C–C–O torsion angle between 163 and −164°, and for 21 structures the O–C–C–O torsion angle was between −26 and 20°, as observed for **3HC-2**. Intermediate torsion angle values in six structures can likely be attributed to packing effects or the steric bulk of substituents (NENLAT −60.2° [24], AHAYEO −47.3° [25], CIVXUC 37.9° [26], SILXAP 49.5° [27], HEJRUL 76.3° [28], DADHOJ 127.2° [29]). The relatively small number of structures with an O–C–C–O torsion angle around 0° prompted us to calculate the optimized structure of the free molecule of **3HC-2** using DFT methods. The minimum energy structure of the free molecule exhibited an O1–C2–C2′–O1′ torsion angle of 0°. Figure 5 shows a superposition of the 3-hydroxychromone moieties of the molecular structure in the crystal and the DFT-optimized molecular structure of the free molecule of **3HC-2**, illustrating the conformational difference between the two structures, which can be attributed to packing effects in the crystal (*vide infra*). A relaxed surface scan was subsequently calculated in order to explore the conformational flexibility of **3HC-2** about the central C2–C2′ bond. This revealed a rotational barrier of ca. 7.5 kcal mol^{-1} and the energy of the s-*trans* conformer was about 1.8 kcal mol^{-1} higher than that of the local ground state structure adopting the s-*cis* conformation (Figure 6).

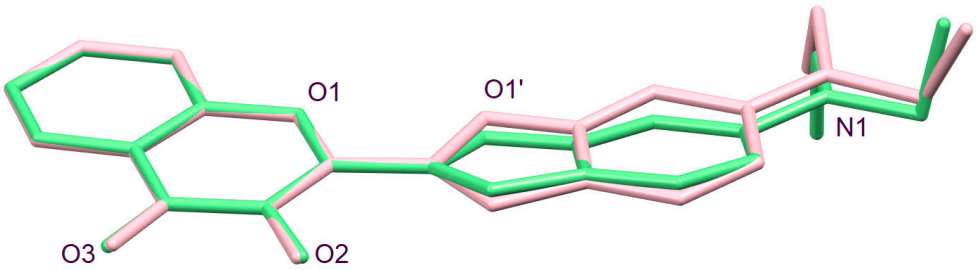

Figure 5. Structure overlay of the 3-hydroxychromone moieties of the molecular structure of the major disorder part structure (green) and DFT-optimized structure (pink) of the free molecule of **3HC-2**.

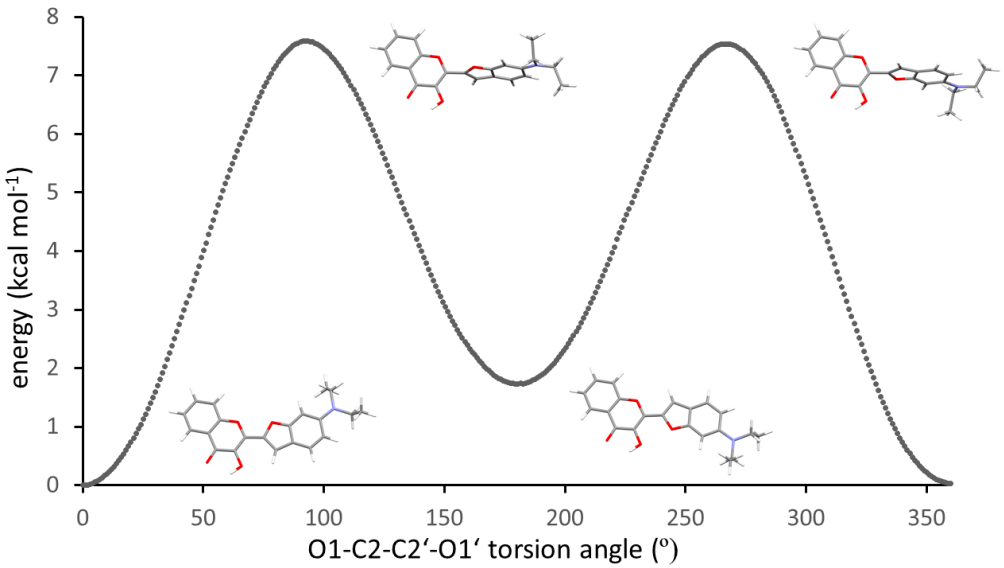

Figure 6. Calculated relaxed surface scan about the central C2–C2′ single bond between the chromenone and benzofuran moieties in **3HC-2**. Color scheme C, grey; H, white; N, blue; O, red.

The supramolecular structure of **3HC-2** in the solid state features centrosymmetric O–H···O hydrogen-bonded dimers (Figure 7). The 3-hydroxy groups each act as a hydrogen bond donor towards the chromone carbonyl oxygen atom of the other molecule in a dimer, resulting in a $R_2^2(10)$ motif [30]. The corresponding hydrogen bond parameters (Table 1) are characteristic of strong hydrogen bonds [31]. The same intermolecular hydrogen bond motif was observed in the crystal structures of the unsubstituted 3-hydroxychromone (HOHHIW) [32] and in the aforementioned IJUCEW and MUGGEC. Whereas the chromone oxygen atom O1 does not exhibit contacts shorter than the sum of van der Waals radii in the crystal, the benzofuran oxygen atom O1′ is approached by a methyl hydrogen atom of the disordered ethyl group of an adjacent molecule. Figure 8 shows the Hirshfeld surface of **3HC-2** and the corresponding 2D fingerprint plot, revealing the dominance of short out of the plane O···H contacts, resulting from the intermolecular O–H···O hydrogen bonding described above and the π···π stacking of the molecules.

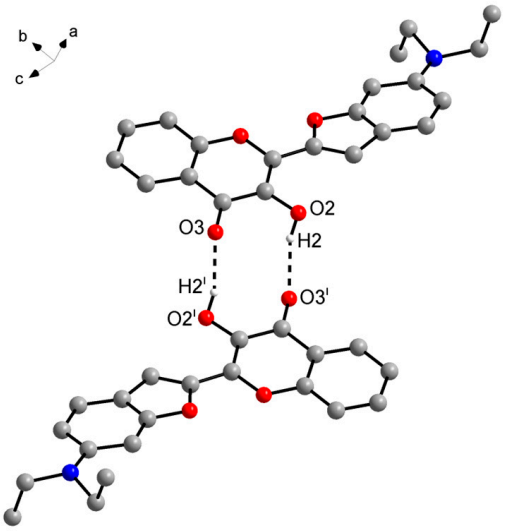

Figure 7. Centrosymmetric hydrogen-bonded dimer of **3HC-2** in the crystal. Dashed lines represent hydrogen bonds. Carbon-bound hydrogen atoms and the minor disorder part are omitted for clarity. Color scheme: C, grey; H, white; N, blue; O, red. Symmetry code: (i) −x, −y, −z + 2.

Table 1. Hydrogen bond geometry for **3HC-2** (Å, °).

D–H···*A* [1]	*d*(*D*–H)	*d*(H···*A*)	*d*(*D*···*A*)	<(*DHA*)
O2–H2···O3^{i}	0.857(14)	1.902(15)	2.7146(13)	157.9(17)

[1] Symmetry code: (i) −x, −y, −z + 2.

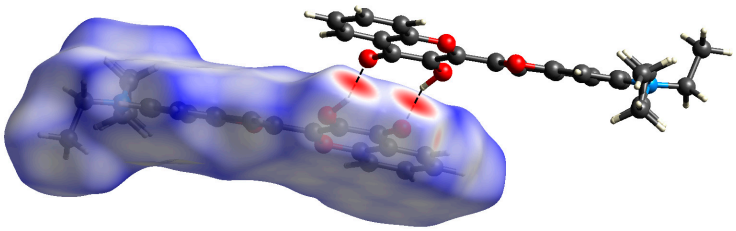

(**a**)

Figure 8. *Cont.*

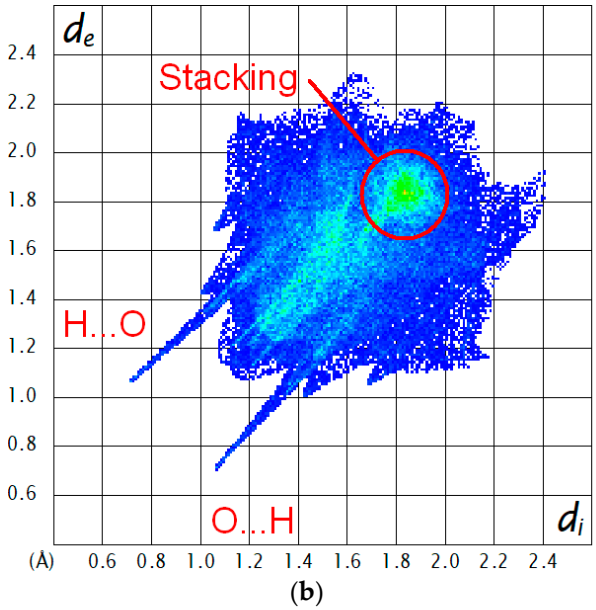

(**b**)

Figure 8. (**a**) Hirshfeld surface mapped with d_{norm} (red areas indicate short contacts) and (**b**) the corresponding 2D fingerprint plot for **3HC-2**; d_i and d_e are the respective interior and exterior distances of the nearest atom to the Hirshfeld surface over the range 0.4–2.6 Å (blue, few points; green, moderate fraction; red, many points). Color scheme for the atoms: C, grey; H, white; N, blue; O, red.

2.2. Labelling of Mycobacterium aurum Cells

The dye trehalose conjugate **3HC-2-Tre** (Figure 2) for the labelling of *M. aurum* cells was prepared from anhydrous trehalose and **3HC-2** as described by Kamariza et al. [5]. In brief, trehalose was brominated in the 6-position by a variation of the Appel reaction using *N*-bromosuccinimide and triphenylphosphine, followed by acetylation. Subsequently, a nucleophilic substitution reaction with **3HC-2**, after deprotonation of the 3-hydroxy group, followed by deacetylation afforded the anticipated **3HC-2-Tre**. We then incubated *M. aurum* cells with 100 µM **3HC-2-Tre** in liquid growth medium for 3 h at 36 °C and subjected the sample to fluorescence microscopy. As shown in Figure 9, our preliminary results demonstrate fluorescence of **3HC-2-Tre**-labelled *M. aurum* cells with λ_{ex} = 485 nm and λ_{em} = 510–531 nm filter sets. It is interesting to note that Kamariza et al. came to the conclusion that **3HC-2-Tre**-labelling of *Mycobacterium smegmatis*, another generally considered non-pathogenic, fast-growing mycobacterium and model organism for the pathogen *M. tuberculosis* [33], was not specific to the trehalose pathway (*vide supra*) [5]. Exploring the mechanism of the labelling of *M. aurum* cells with **3HC-2-Tre**, however, is beyond the scope of this preliminary investigation.

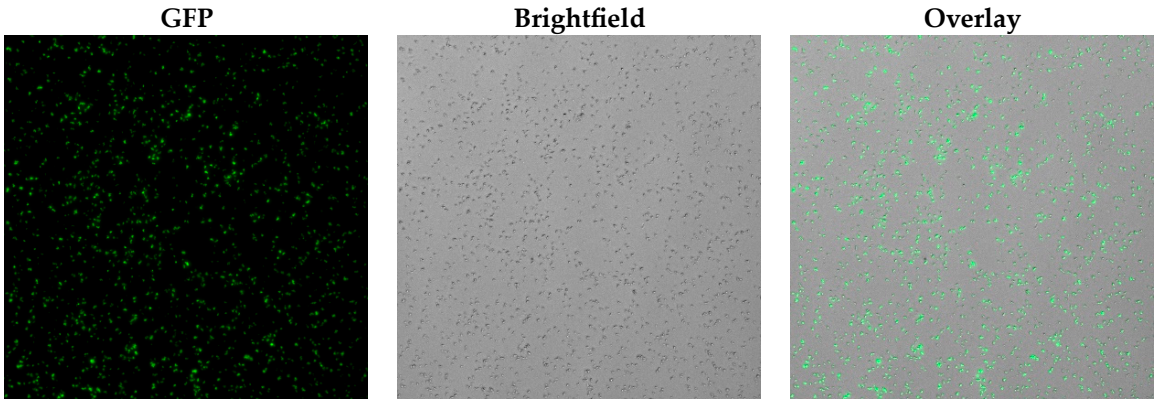

Figure 9. Microscope imaging (20× magnification) of *M. aurum* cells treated with 100 µM **3HC-2-Tre** (GFP channel: λ_{ex} = 485 nm, λ_{em} = 510–531 nm).

3. Materials and Methods

3.1. General

Compounds **3HC-2** and **3HC-2-Tre** were prepared following the procedures reported by Kamariza et al. [5]. The synthesis of the aldehyde precursor to **3HC-2**, i.e., 6-(diethylamino)benzofuran-2-carbaldehyde, from 3-dimethylaminophenol is described in Ref. [16]. Experimental details of the preparation of **3HC-2-Tre** can be found in the Supplementary Materials. The starting materials 3-dimethylaminophenol (97.69%, BLD Pharmatech GmbH, Kaiserslautern, Germany), 2′-hydroxyacetophenone (99.94%, BLD Pharmatech GmbH), and anhydrous trehalose (>98.0%, TCI, Chuo-ku, Tokyo) were purchased and used as received.

3.2. X-ray Crystallography

A few crystals of **3HC-2** suitable for single-crystal X-ray diffraction were obtained by chance when the remainder of a heptane/ethyl acetate solution resulting from flash chromatography evaporated to dryness in a tube. The crystals were coated with perfluoropolyether PFO-XR75 and mounted using a MiTeGen cryo-loop. The X-ray diffraction data were measured on a Bruker AXS D8 Venture diffractometer, equipped with an Incoatec IμS Diamond microfocus X-ray source, Incoatec multilayer optics, and a CMOS Photon III detector. The APEX4 software was used to control the diffractometer [34]. The raw data were processed with the SAINT software [35] and corrected for absorption effects with SADABS-2016/2 [36] using the Gaussian method based on indexed crystal faces.

The crystal structure was solved with SHELXT [37] and refined with SHELXL-2019/3 [38]. Anisotropic atomic displacement parameters (ADPs) were introduced for all non-hydrogen atoms. The diethylamino group was affected by positional disorder, which was taken into account by a split model for one ethyl group. Refinement of the ratio of occupancies by means of a free variable resulted in 0.531(4):0.469(4). Similar distance (SADI) and enhanced rigid-bond restraints (RIGU) [39] were applied to the disordered ethyl group. Except for the hydroxy hydrogen atom H2 and H3′ on the benzofuran moiety, hydrogen atoms were placed in geometrically calculated positions with C_{aromat}–H = 0.95 Å, $C_{methylene}$–H = 0.99 Å, and C_{methyl}–H = 0.98 Å and refined using a riding model with U_{iso}(H) = 1.2 U_{eq}(C) (1.5 for methyl groups). The initial torsion angle of the methyl group of C10 was determined in a circular Fourier calculation and subsequently refined while maintaining a tetrahedral structure. H2 and H3′ were located in difference Fourier maps and refined with the O2–H2 and C3′–H3′ distance restrained to target values of 0.84(2) and 0.95(2) Å, respectively, and with U_{iso}(H) = 1.2 U_{eq}(C, O). Crystal data and refinement details are listed in Table 2. Structure pictures were drawn with Diamond [40]. Hirshfeld surface analysis was carried out using CrystalExplorer [41].

3.3. Computational Methods

DFT calculations were performed with ORCA (version 5.0) [42] with a B3LYP/G VWN1 hybrid functional (20% HF exchange) [43–45], using a def2-TZVPP basis set [45]. Optimization of the structure was completed using the BFGS method from an initial Hessian according to Almoef's model with a very tight self-consistent field convergence threshold [46]. Calculations were made on the free molecule of **3HC-2**. A relaxed surface scan was carried out varying the crystallographic O1–C2–C2′–O1′ torsion angle from 0 to 359° in 1° steps using a def2-TZVPP basis set and optimizing as above with a tight self-consistent field convergence criterion. Structures near the transition states were subsequently optimized using a def2-TZVPP basis set and a very tight self-consistent field convergence criterion, as for the optimized structure. The optimized local minimum-energy structures exhibited only positive modes and the transition states each exhibited one imaginary mode. Cartesian coordinates of the DFT-optimized structure of **3HC-2** can be found in the Supplementary Materials. Structure pictures were generated with Mercury [47].

Table 2. Crystal data and refinement details for **3HC-2**.

Empirical Formula	$C_{21}H_{19}NO_4$
M_r	349.37
T (K)	100(2)
λ (Å)	0.71073
Crystal system, space group	Triclinic, *P*-1
a (Å)	7.2022(5)
b (Å)	8.4003(5)
c (Å)	15.0621(10)
α (°)	99.969(4)
β (°)	94.673(4)
γ (°)	111.188(2)
V (Å^3)	826.48(9)
Z, ρ_{calc} (g cm^{-3})	2, 1.404
μ_{calc} (mm^{-1})	0.098
F(000)	368
Crystal size (mm)	0.236 × 0.112 × 0.020
θ range (°)	2.665–30.555
Reflections collected/unique	91202/5061
R_{int}	0.0553
Observed reflections [$I > 2\sigma(I)$]	3946
Data/restraints/parameters	5061/29/261
Goodness-of-fit on F^2	1.027
$R1$ [$I > 2\sigma(I)$]	0.0483
$wR2$ (all data)	0.1418
$\Delta\rho_{max}$, $\Delta\rho_{min}$	0.471/−0.556

3.4. Microbiology

M. aurum DSM 43999 was cultivated via the inoculation of a single colony from a fresh streak plate (Middlebrook 7H10 agar) into 10 mL of Middlebrook 7H9 liquid medium supplemented with 10% ADS [5% (*m*/*v*) bovine serum albumin fraction V, 0.81% (*m*/*v*) sodium chloride, 2% (*m*/*v*) dextrose in purified water] and 0.05% polysorbate 80. The culture was grown to an OD_{600} between 0.2 and 0.8 for the labelling experiment by incubation at 36 °C with shaking (50 rpm). After dilution to an initial concentration of 5×10^7 CFU/mL (OD_{600} 0.1 = 1×10^8 CFU/mL) with growth medium, the culture was transferred to a clear flat-bottom 96-well plate (Sarstedt, 83.3924.500) with 100 µL per well. Subsequently, 1 µL of **3HC-2-Tre** (10 mM in DMSO) was added to each well to achieve a final dye concentration of 100 µM. After homogenization by pipetting, the plate was incubated for 3 h at 36 °C with shaking (50 rpm).

3.5. Fluorescence Microscopy

After incubation (see Section 3.4), the contents of the wells were homogenized by pipetting and 1 µL of each well was transferred to a black clear flat-bottom 96-well plate (Greiner bio one, 6550909) filled with 200 µL phosphate-buffered saline per well. Fluorescence microcopy was performed with a Thermo Scientific (Waltham, MA, USA) CellInsight CX5 instrument. Samples were excited at 485 nm and imaged with the GFP channel (510–531 nm).

4. Conclusions

We have structurally characterized the 3-hydroxychromone dye **3HC-2** in the solid state by X-ray crystallography. In the crystal, the molecule exhibits an s-*cis* conformation with an O–C–C–O torsion angle of ±13.76(16)°. DFT calculations on the free molecule gave an O–C–C–O torsion angle of ca. 0°, and revealed that the s-*cis* conformer was approximately 1.8 kcal mol^{-1} more stable than the s-*trans* conformer, with a rotational barrier of ca. 7.5 kcal mol^{-1}. Preliminary labelling experiments demonstrated that *M. aurum* cells incubated in the presence of the dye trehalose conjugate **3HC-2-Tre** could be detected by fluorescence microscopy in the GFP channel. We expect that this will facilitate in vitro testing of new antimycobacterial agents using this test bacterium, which is generally regarded as non-pathogenic.

Supplementary Materials: The following materials are available online: Description of the synthesis of **3HC-2-Tre** and cartesian coordinates of the DFT-optimized structures of the s-*cis* and s-*trans* conformers of **3HC-2**.

Author Contributions: Conceptualization, A.R. and R.W.S.; methodology, A.R., R.G., F.S., L.M. and R.W.S.; validation, A.R., R.G., F.S., L.M. and R.W.S.; formal analysis, A.R., R.G., F.S., L.M. and R.W.S.; investigation, A.R., R.G., F.S. and L.M.; resources, A.R. and R.G.; data curation, R.W.S.; writing—original draft preparation, F.S. and R.W.S.; writing—review and editing, A.R., R.G. and L.M.; visualization, A.R., R.G., F.S., L.M. and R.W.S.; supervision, A.R.; project administration, A.R. and R.W.S.; funding acquisition, A.R. and F.S. All authors have read and agreed to the published version of the manuscript.

Funding: This work was funded by the Deutsche Forschungsgemeinschaft (DFG, German Research Foundation)—432291016 (to A.R.), Mukoviszidose Institut gGmbH (Bonn, Germany) project number 2202 (to A.R.), the research and development arm of the German Cystic Fibrosis Association Mukoviszidose e. V. and by a scholarship from the Vereinigung der Freunde und Förderer des Institutes für Pharmazie der Martin-Luther-Universität Halle-Wittenberg (VFFIP) to F.S.

Data Availability Statement: CCDC 2258616 contains the supplementary crystallographic data for this paper. The data can be obtained free of charge from the Cambridge Crystallographic Data Centre via www.ccdc.cam.ac.uk/structures. Cartesian coordinates of the DFT-calculated s-*cis* and s-*trans* conformers of **3HC-2** can be found in the Supplementary Materials.

Acknowledgments: We would like to thank Christian W. Lehmann for providing access to the X-ray diffraction facility at the Max-Planck-Institut für Kohlenforschung and Heike Schucht for technical assistance with the X-ray intensity data collection.

Conflicts of Interest: The authors declare no conflict of interest. The funders had no role in the design of the study; in the collection, analyses, or interpretation of data; in the writing of the manuscript; or in the decision to publish the results.

Sample Availability: Not Applicable.

References

1. World Health Organization. *Global Tuberculosis Report 2022*; World Health Organization: Geneva, Switzerland, 2022.
2. To, K.; Cao, R.; Yegiazaryan, A.; Owens, J.; Venketaraman, V. General Overview of Nontuberculous Mycobacteria Opportunistic Pathogens: *Mycobacterium avium* and *Mycobacterium abscessus*. *J. Clin. Med.* **2020**, *9*, 2541. [CrossRef] [PubMed]
3. Dahl, V.N.; Molhave, M.; Floe, A.; van Ingen, J.; Schon, T.; Lillebaek, T.; Andersen, A.B.; Wejse, C. Global trends of pulmonary infections with nontuberculous mycobacteria: A systematic review. *Int. J. Infect. Dis.* **2022**, *125*, 120–131. [CrossRef]
4. Singhal, R.; Myneedu, V.P. Microscopy as a diagnostic tool in pulmonary tuberculosis. *Int. J. Mycobacteriology* **2015**, *4*, 1–6. [CrossRef] [PubMed]
5. Kamariza, M.; Keyser, S.G.L.; Utz, A.; Knapp, B.D.; Ealand, C.; Ahn, G.; Cambier, C.J.; Chen, T.; Kana, B.; Huang, K.C.; et al. Toward Point-of-Care Detection of *Mycobacterium tuberculosis*: A Brighter Solvatochromic Probe Detects Mycobacteria within Minutes. *JACS Au.* **2021**, *1*, 1368–1379. [CrossRef] [PubMed]
6. Tortoli, E.; Brown-Elliott, B.A.; Chalmers, J.D.; Cirillo, D.M.; Daley, C.L.; Emler, S.; Floto, R.A.; Garcia, M.J.; Hoefsloot, W.; Koh, W.-J.; et al. Same meat, different gravy: Ignore the new names of mycobacteria. *Eur. Respir. J.* **2019**, *54*, 1900795. *Mycobacterium aurum* has been reclassified into the new genus *Mycolicibacterium*, but the new names of mycobacteria have not widely been accepted. [CrossRef] [PubMed]

7. Phelan, J.; Maitra, A.; McNerney, R.; Nair, M.; Gupta, A.; Coll, F.; Pain, A.; Bhakta, S.; Clark, T.G. The draft genome of *Mycobacterium aurum*, a potential model organism for investigating drugs against *Mycobacterium tuberculosis* and *Mycobacterium leprae*. *Int. J. Mycobacteriology* **2015**, *4*, 207–216. [CrossRef] [PubMed]
8. Namouchi, A.; Cimino, M.; Favre-Rochex, S.; Charles, P.; Gicquel, B. Phenotypic and genomic comparison of Mycobacterium aurum and surrogate model species to *Mycobacterium tuberculosis*: Implications for drug discovery. *BMC Genom.* **2017**, *18*, 530. [CrossRef]
9. Gupta, A.; Bhakta, S.; Kundu, S.; Gupta, M.; Srivastava, B.S.; Srivastava, R. Fast-growing, non-infectious and intracellularly surviving drug-resistant *Mycobacterium aurum*: A model for high-throughput antituberculosis drug screening. *J. Antimicrob. Chemother.* **2009**, *64*, 774–781. [CrossRef]
10. Sood, S.; Yadav, A.; Shrivastava, R. *Mycobacterium aurum* is Unable to Survive *Mycobacterium tuberculosis* Latency Associated Stress Conditions: Implications as Non-suitable Model Organism. *Indian J. Microbiol.* **2016**, *56*, 198–204. [CrossRef]
11. Honarvar, B.; Movahedan, H.; Mahmoodi, M.; Sheikholeslami, F.M.; Farnia, P. *Mycobacterium aurum* keratitis: An unusual etiology of a sight-threatening infection. *Braz. J. Infect. Dis.* **2012**, *16*, 204–208. [CrossRef]
12. Madikizela, B.; Eckhardt, T.; Goddard, R.; Richter, A.; Lins, A.; Lehmann, C.; Imming, P.; Seidel, R.W. Synthesis, structural characterization and antimycobacterial evaluation of several halogenated non-nitro benzothiazinones. *Med. Chem. Res.* **2021**, *30*, 1523–1533. [CrossRef] [PubMed]
13. Eckhardt, T.; Goddard, R.; Lehmann, C.; Richter, A.; Sahile, H.A.; Liu, R.; Tiwari, R.; Oliver, A.G.; Miller, M.J.; Seidel, R.W.; et al. Crystallographic evidence for unintended benzisothiazolinone 1-oxide formation from benzothiazinones through oxidation. *Acta Crystallogr. Sect. C* **2020**, *76*, 907–913. [CrossRef] [PubMed]
14. Richter, A.; Seidel, R.W.; Goddard, R.; Eckhardt, T.; Lehmann, C.; Dörner, J.; Siersleben, F.; Sondermann, T.; Mann, L.; Patzer, M.; et al. BTZ-Derived Benzisothiazolinones with In Vitro Activity against *Mycobacterium tuberculosis*. *ACS Med. Chem. Lett.* **2022**, *13*, 1302–1310. [CrossRef] [PubMed]
15. Klymchenko, A.S.; Ozturk, T.; Pivovarenko, V.G.; Demchenko, A.P. A 3-hydroxychromone with dramatically improved fluorescence properties. *Tetrahedron Lett.* **2001**, *42*, 7967–7970. [CrossRef]
16. Klymchenko, A.S.; Pivovarenko, V.G.; Ozturk, T.; Demchenko, A.P. Modulation of the solvent-dependent dual emission in 3-hydroxychromones by substituents. *New J. Chem.* **2003**, *27*, 1336–1343. [CrossRef]
17. Groom, C.R.; Bruno, I.J.; Lightfoot, M.P.; Ward, S.C. The Cambridge Structural Database. *Acta Crystallogr. Sect. B* **2016**, *72*, 171–179. [CrossRef]
18. Thomas, I.R.; Bruno, I.J.; Cole, J.C.; Macrae, C.F.; Pidcock, E.; Wood, P.A. WebCSD: The online portal to the Cambridge Structural Database. *J. Appl. Crystallogr.* **2010**, *43*, 362–366. [CrossRef]
19. Wera, M.; Pivovarenko, V.G.; Sikorski, A.; Lis, T.; Blazejowski, J. 2-(Furan-2-yl)-3-hydroxy-4H-chromen-4-one. *Acta Crystallogr. Sect. E* **2011**, *67*, o266. [CrossRef]
20. Camargo, M.L.M.; dos Santos, F.A.; Pizzuti, L.; Abram, U.; Schwade, V.D. Complexes with Furyl-Substituted 3-Hydroxychromone: Synthesis, Characterization and Fluorescence Studies. *J. Braz. Chem. Soc.* **2021**, *32*, 1519–1530. [CrossRef]
21. Camargo, M.L.M.; Schwalm, C.S.; Bortolotto, T.; de Freitas Daudt, N.; Rossi, G.G.; Anraku de Campos, M.M.; D'Oliveira, K.A.; Cuin, A.; Schwade, V.D. M^{II} (M = Mn, Fe, Co, Ni and Cu) complexes with a chromone-derived neutral ligand: Synthesis, structural characterization, photocatalytic and mycobacterial activity studies. *New J. Chem.* **2022**, *46*, 2534–2545. [CrossRef]
22. Tseng, H.-W.; Shen, J.-Y.; Kuo, T.-Y.; Tu, T.-S.; Chen, Y.-A.; Demchenko, A.P.; Chou, P.-T. Excited-state intramolecular proton-transfer reaction demonstrating anti-Kasha behavior. *Chem. Sci.* **2016**, *7*, 655–665. [CrossRef] [PubMed]
23. Mughal, E.U.; Javid, A.; Sadiq, A.; Murtaza, S.; Zafar, M.N.; Khan, B.A.; Sumrra, S.H.; Tahir, M.N.; Kanwal; Khan, K.M. Synthesis, structure-activity relationship and molecular docking studies of 3-O-flavonol glycosides as cholinesterase inhibitors. *Bioorganic Med. Chem.* **2018**, *26*, 3696–3706. [CrossRef] [PubMed]
24. Peters, E.-M.; Peters, K.; Meints, C.; Tochtermann, W. Crystal structure of (pM*,pM*)-(±)-bi-(dimethyl-3,6-decanooxepine-4,5-dicarboxylate), $[C_6HO(CH_2)IO(COOCH_3)_2]_2$. *Z. Für Krist.-New Cryst. Struct.* **2001**, *216*, 315–316. [CrossRef]
25. Alcaide, B.; Almendros, P.; Carrascosa, R.; Torres, M.R. Synthesis of a New Class of C_2-Symmetrical Biheteroaryls by Ammonium Cerium(IV) Nitrate Mediated Dimerization of 2-(Furan-3-yl)pyrroles. *Eur. J. Org. Chem.* **2010**, *2010*, 823–826. [CrossRef]
26. Fan, Y.-S.; Das, U.; Hsiao, M.-Y.; Liu, M.-H.; Lin, W. Chemoselective Intramolecular Wittig Reactions for the Synthesis of Oxazoles and Benzofurans. *J. Org. Chem.* **2014**, *79*, 11567–11582. [CrossRef]
27. Mulay, S.V.; Bogoslavky, B.; Galanti, I.; Galun, E.; Gidron, O. Bifuran-imide: A stable furan building unit for organic electronics. *J. Mater. Chem. C* **2018**, *6*, 11951–11955. [CrossRef]
28. Ookubo, Y.; Wakamiya, A.; Yorimitsu, H.; Osuka, A. Synthesis of a Library of Fluorescent 2-Aryl-3-trifluoromethylnaphthofurans from Naphthols by Using a Sequential Pummerer-Annulation/Cross-Coupling Strategy and their Photophysical Properties. *Chem. A Eur. J.* **2012**, *18*, 12690–12697. [CrossRef]
29. Wang, C.-H.; Gao, Z.-C.; Sun, W.; Guo, X.; Zhang, F.-B. P···O noncovalent conformational locks for constructing highly planar Bis(diphenylphosphanyl) Bi(benzofurano). *Dye. Pigment.* **2021**, *184*, 108820. [CrossRef]
30. Bernstein, J.; Davis, R.E.; Shimoni, L.; Chang, N.L. Patterns in Hydrogen Bonding: Functionality and Graph Set Analysis in Crystals. *Angew. Chem. Int. Ed.* **1995**, *34*, 1555–1573. [CrossRef]
31. Thakuria, R.; Sarma, B.; Nangia, A. 7.03-Hydrogen Bonding in Molecular Crystals. In *Comprehensive Supramolecular Chemistry II*; Atwood, J.L., Ed.; Elsevier: Oxford, UK, 2017; pp. 25–48. [CrossRef]

32. Binbuga, N.; Schultz, T.P.; Henry, W.P. Intra- and intermolecular hydrogen bonding in 3-hydroxy- and 5-hydroxychromone. *Tetrahedron Lett.* **2008**, *49*, 5762–5765. [CrossRef]
33. T, J.A.S.; J, R.; Rajan, A.; Shankar, V. Features of the biochemistry of *Mycobacterium smegmatis*, as a possible model for *Mycobacterium tuberculosis*. *J. Infect. Public Health* **2020**, *13*, 1255–1264. [CrossRef] [PubMed]
34. *APEX4*; Bruker AXS Inc.: Madison, WI, USA, 2017.
35. *SAINT*; Bruker AXS Inc.: Madison, WI, USA, 2012.
36. *SADABS*; Bruker AXS Inc.: Madison, WI, USA, 2012.
37. Sheldrick, G.M. SHELXT-integrated space-group and crystal-structure determination. *Acta Crystallogr. Sect. A* **2015**, *71*, 3–8. [CrossRef] [PubMed]
38. Sheldrick, G.M. Crystal structure refinement with SHELXL. *Acta Crystallogr. Sect. C* **2015**, *71*, 3–8. [CrossRef] [PubMed]
39. Thorn, A.; Dittrich, B.; Sheldrick, G.M. Enhanced rigid-bond restraints. *Acta Crystallogr. Sect. A* **2012**, *68*, 448–451. [CrossRef]
40. Brandenburg, K. *Diamond*; Crystal Impact GbR: Bonn, Germany, 2018.
41. Spackman, P.R.; Turner, M.J.; McKinnon, J.J.; Wolff, S.K.; Grimwood, D.J.; Jayatilaka, D.; Spackman, M.A. CrystalExplorer: A program for Hirshfeld surface analysis, visualization and quantitative analysis of molecular crystals. *J. Appl. Crystallogr.* **2021**, *54*, 1006–1011. [CrossRef]
42. Neese, F.; Wennmohs, F.; Becker, U.; Riplinger, C. The ORCA quantum chemistry program package. *J. Chem. Phys.* **2020**, *152*, 224108. [CrossRef]
43. Becke, A.D. Density-functional thermochemistry. III. The role of exact exchange. *J. Chem. Phys.* **1993**, *98*, 5648–5652. [CrossRef]
44. Hertwig, R.H.; Koch, W. On the parameterization of the local correlation functional. What is Becke-3-LYP? *Chem. Phys. Lett.* **1997**, *268*, 345–351. [CrossRef]
45. Weigend, F.; Ahlrichs, R. Balanced basis sets of split valence, triple zeta valence and quadruple zeta valence quality for H to Rn: Design and assessment of accuracy. *Phys. Chem. Chem. Phys.* **2005**, *7*, 3297–3305. [CrossRef]
46. Fletcher, R. *Practical Methods of Optimization*, 2nd ed.; John Wiley & Sons: Hoboken, NJ, USA, 2000.
47. Macrae, C.F.; Sovago, I.; Cottrell, S.J.; Galek, P.T.A.; McCabe, P.; Pidcock, E.; Platings, M.; Shields, G.P.; Stevens, J.S.; Towler, M.; et al. Mercury 4.0: From visualization to analysis, design and prediction. *J. Appl. Crystallogr.* **2020**, *53*, 226–235. [CrossRef]